ACS OMEGA

http://pubs.acs.org/journal/acsodf

Article

NiCoP with Dandelion-like Arrays Anchored on Nanowires for Electrocatalytic Overall Water Splitting

Wei Pang, Ailing Fan,* Yaqi Guo, Dengkui Xie, and Dianchao Gao

Cite This: *ACS Omega* 2021, 6, 26822−26828

Read Online

ACCESS | Metrics & More | Article Recommendations | Supporting Information

ABSTRACT: Although transition-metal-based phosphides as cost-effective catalysts have great potential for transforming water to hydrogen, their electrocatalytic property for industrial application is still limited. Herein, we focus on developing amorphous NiCoP with dandelion-like arrays anchored on nanowires through a universal strategy of hydrothermal and phosphorization. The hierarchical structure features in larger catalytic surface areas expedited reaction kinetics and improved structural stability. Benefiting from these merits, the NiCoP reaches 10 mA cm^{-2} at an overpotential of mere 57 mV for a hydrogen evolution reaction in standard solution. Also, a profound activity for the generation of oxygen is along with it, which requires 276 mV to attain 10 mA cm^{-2}. Moreover, it demonstrates satisfying durability for both processes.

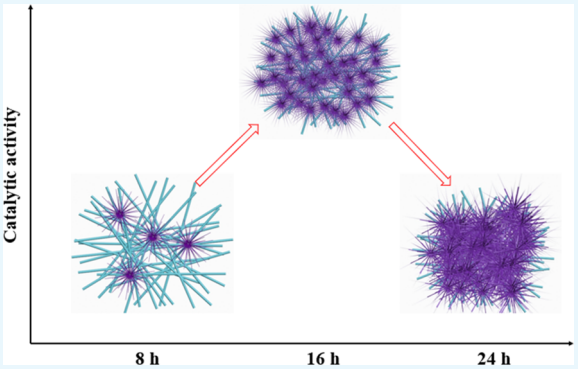

INTRODUCTION

Taking advantage of renewable energies to generate hydrogen (H_2) from water is greatly viewed as a promising strategy for reducing fossil dependence.[1] However, the conversion efficiency is restricted by the two half reactions of hydrogen and oxygen. Currently, both processes mainly rely on the precious materials Pt or RuO_2 to reduce the reaction barrier and expedite the sluggish kinetics.[2] However, the rare materials with expensive costs cannot meet the requirement of practical application. Thus, developing cost-efficient and robust alternatives toward high-efficiency water splitting attracts enormous research efforts and exists still as a bottle-neck technique.

To replace noble catalysts, numerous studies focus on electrocatalysts with low cost, good catalytic activity, and easy processing. For example, considerable achievements have been reported on various transition-metal-based compounds,[3−28] including selenides, sulfides, nitrides, etc. Among them, transition-metal-based phosphides (TMPs) have outstood with their intrinsic high catalytic activities, high stability, and good conductivity toward overall water splitting in alkaline solutions.[29−38] Further, introducing other metals to TMPs has been proposed.[39] For instance, adjusting the composition of Ni_2P with Co doping, the bimetal phosphides exhibit advantageous electrocatalytic performance to the monometallic counterparts and many other bimetallic alloying phosphides due to synergistic effects.[40,41] Accordingly, some investigations have been dedicated to regulate chemical compositions to improve the activity of TMP electrocatalysts.[42−46]

Structure optimizing offers an additional strategy to enhance the property by constructing and exposing more active sites.[47] Catalysts with different morphologies from 0D to 2D have been reported.[48−50] These materials generally provide a large active area and show the advantages for electron transfer and diffusion of electrolytes. However, their durability is unsatisfying due to easy agglomeration.[43] Therefore, 3D nanocatalysts with a hierarchical structure and superior stability become highly desirable.[51−55]

Here, we develop NiCoP with dandelion-like arrays anchored on nanowires by a universal scheme of hydrothermal and phosphorization. The unique structure demonstrates excellent activity for hydrogen evolution reaction (HER) and oxygen evolution reaction (OER) in alkaline solution. After experiencing electrocatalysis for over 10 h, the catalyst retains the dandelion-like morphology well, demonstrating its outstanding mechanical stability. Furthermore, they show an impressive property when they act as couple electrodes for overall water splitting. All the merits endow the hierarchical NiCoP with a promise for practical application.

RESULTS AND DISCUSSION

Hierarchical NiCoP with dandelion-like arrays anchored on nanowires was synthesized by a facile hydrothermal, phosphorization strategy, as illustrated in Figure S1. In brief, a hydrothermal method was adopted to obtain the NiCo-pre,

Received: March 30, 2021
Accepted: September 10, 2021
Published: October 11, 2021

which is grown on commercial Ni foam, followed by phosphorization to receive the final 3D NiCoP nanostructures.

The phase of the catalyst is identified by XRD. As shown in Figure S2, besides the three sharp diffraction peaks belonging to the Ni foam, the XRD pattern indicates a set of relatively weak peaks, which can be assigned to the phase of NiCoP (JCPDS, #71-2336). The SEM images of the prepared NiCoP with dandelion-like arrays in a uniform size of about 6 μm anchored on nanowires are depicted in Figure 1a. As can be

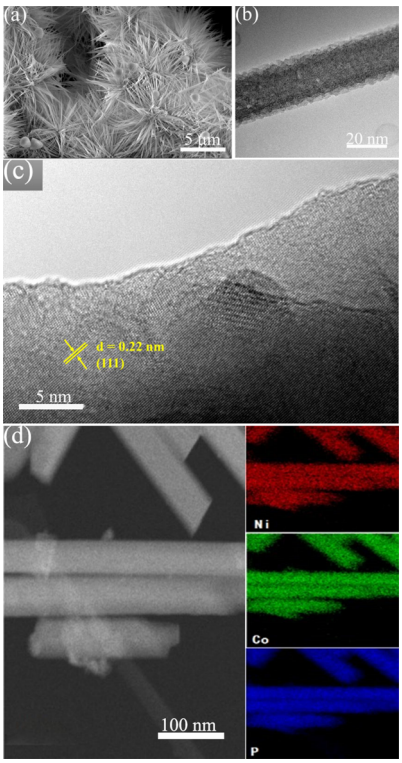

Figure 1. (a) SEM, (b) TEM, (c) and HRTEM images of NiCoP and (d) elemental mapping of Ni, Co, and P.

seen, the dandelion-like arrays are made of numerous and interconnected nanowires, forming a hierarchical and loose structure. Such a well-aligned structure could reduce the stacking of the catalysts, favorably improving the accessibility of the reactant to active sites and exposing more active sites. In addition, the nanowire feature can absorb a liquid electrolyte on the catalyst surface due to the strong capillary forces. In consequence, it will promote the release of hydrogen bubbles from the electrocatalyst surface and reduce the gas−solid friction, which is essential for both HER and OER. Figure 1b shows a TEM image of a nanowire in the dandelion-like arrays. It depicts that the nanowire with a convex surface comprises numerous nanocrystals. This may be due to the fact that the P/O or P/OH (−O or−−OH originating from a precursor) exchange process leads to the formation of coarse phosphide nanocrystals during phosphorization, which would further increase the effective surface areas of the catalyst. Additionally, the HRTEM image (Figure 1c) shows an interplanar spacing of 0.22 nm belonging to (111) facets of the NiCoP phase. Furthermore, the Ni, Co, and P elements are distributed uniformly over the nanowires according to the energy-dispersive X-ray spectroscopy (EDS) elemental maps (Figure 1d).

During phosphorization, the NiCoP inherits the dandelion-like morphology of the NiCo-pre well. As shown in Figure 2−

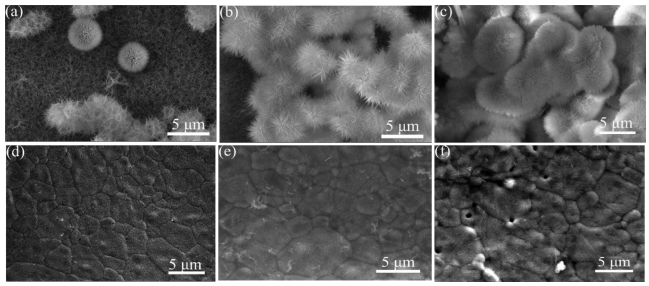

Figure 2. SEM images of NiCo-pre obtained at (a) 8 h, (b) 16 h, and (c) 24 h and NiCo-pre/4 obtained at (d) 8 h, (e) 16 h, and (f) 24 h.

ca, the precursor with dandelion-like arrays anchored on nanowires was prepared at different reaction times. When the reaction time is 8 h, a small amount of precipitates is obtained, showing that nanowires first form on the surface of Ni foam, and then part of nanowires forms dandelion-like arrays by self-assembling (Figure 2a). The SEM images of the evolution from nanowires to dandelion-like arrays at different magnifications are clearly shown in Figure S3a,b. We speculate that the unique structure will greatly enlarge the active surface area and avoid the agglomeration of catalysts. Extending the reaction time to 16 h, a large number of dandelion-like arrays are formed by nanowires (Figure 2b). Elongating the reaction time to 24 h, the dandelion-like arrays are obtained with an enhanced yield, as illustrated in Figure 2c. They densely assemble and completely cover the nanowires initially grown on the foam. In addition, the single dandelion-like array is denser itself. Spaces among the nanowires composing the dandelion-like array are almost invisible. We assume that the loose and dense dandelion-like arrays will result in different activities because the dense dandelion-like arrays plague the contact of reactants to active sites and subsequently affect the electrocatalytic activity. Furthermore, it is interesting that the NiCo-pre film is formed on the surface of Ni foam under a relatively low (quarter) concentration of the solution (Figure 2−fd). The surface of the NiCo-pre/4 film becomes coarse with an extended hydrothermal reaction time. This phenomenon may be related to the hydroxyl and nitrate ions. We assume that the hydroxyl and nitrate ions from the hydrolysis of salt/urea during the hydrothermal reaction not only participate in the formation of the precursor and promote the anisotropic growth of the nanowires but also serve as coordination agents that are profitable to form more intricate hierarchical structures at a high solution concentration.

The surface chemical states of the NiCoP were further analyzed by X-ray photoelectron spectroscopy (XPS). The valence states and local environment of Ni, Co, and P centers have great impact on the electrocatalyst activities according to previous reports. As depicted in Figure 3a, at the binding energies of 857.6 and 862.8 eV, the spectrum of Ni $2p_{3/2}$ of the precursor exhibits two main peaks that can be assigned to $Ni(OH)_x$ and its satellite peak. At the binding energies of 853.0, 856.5, and 861.6 eV, we can find three peaks appear after phosphorization. The sharp peak that is near to that of metallic Ni (852.6 eV) at 853.0 eV can be assigned to the P−Ni bond, implying the partially charged Ni species ($Ni^{\delta+}$) exist. The binding energies of 856.5 and 861.6 eV can be assigned to $Ni-PO_x$ (Ni^{2+}) and its shake up satellite, respectively. The Ni

https://doi.org/10.1021/acsomega.1c01650
ACS Omega 2021, 6, 26822−26828

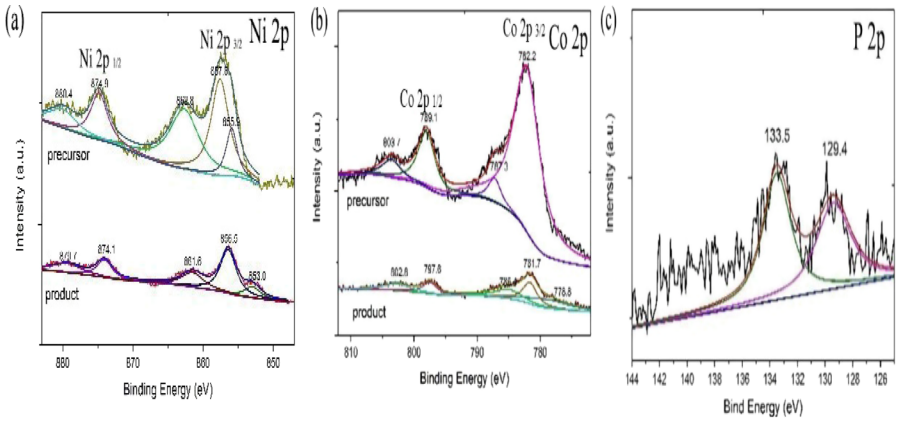

Figure 3. High-resolution XPS spectra of precursors and NiCoP: (a) Ni 2p, (b) Co 2p, and (c) P 2p.

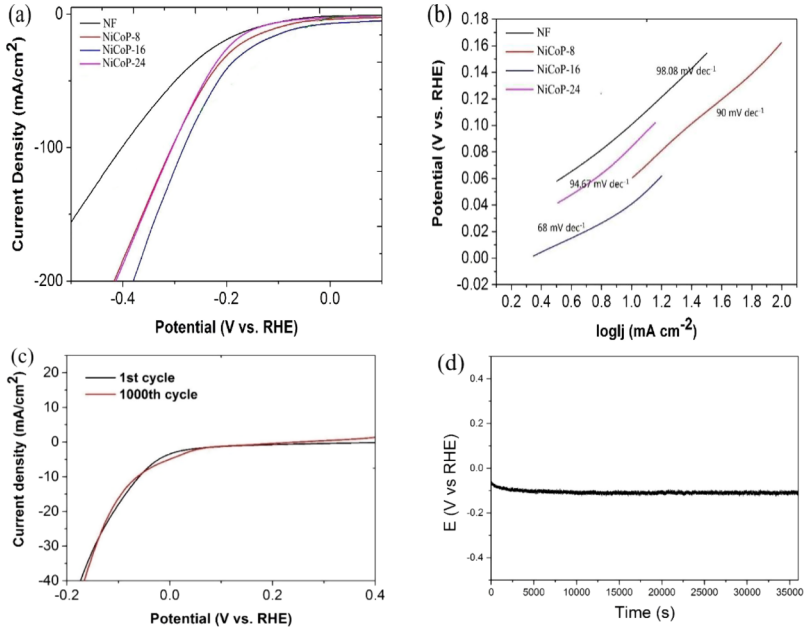

Figure 4. HER activity of the as-prepared NiCoP in H_2-saturated 1 M KOH. (a) Polarization curves recorded with a scan rate of 5 mV s^{-1}. (b) Tafel plots derived from (a). (c) HER stability test of NiCoP-16 for 1000 potential cycles. (d) CP curves of NiCoP-16.

$2p_{1/2}$ region also shows a peak at 874.9 eV (Ni^{2+}) and one satellite peak at 880.4 ($Ni^{\delta+}$) eV. Similar to this, the Co $2p_{3/2}$ core-level spectrum (Figure 3b) exhibits a satellite peak at 785.4 eV, an oxidized Co−PO_x (Co^{2+}) peak at 781.7 eV, and a positively charged Co−P species ($Co^{\delta+}$) at 778.8 eV.[56] The peaks at 798.1 and 802.8 eV belong to Co $2p_{1/2}$, which are oxidized Co species (Co^{2+}), and the satellite, respectively. The P 2p region was exhibited in Figure 3c, in which the binding energies at 129.4 and 133.5 eV of two doublets can be witnessed. The formation of metal-P and the latter to phosphate species may be due to air exposure according to the former peak.[56] According to the peak at 129.4 eV, the partial P is negatively charged, which is slightly lower than that of elemental P (130 eV).[40] On the whole, the opposite shifts between P 2p, Ni 2p, and Co 2p are mainly attributed to partial electron transfer. The negative shift of P 2p and the positive shifts of Ni and Co 2p reveal the enhanced electron transfer capacity from metallic Ni and Co to P, resulting in a hydride acceptor (Ni and Co sites) and proton acceptor (P site), respectively, and subsequently stimulating an adsorption and desorption process.[57]

We then evaluated HER performance of the dandelion-like NiCoP sample in 1 M KOH in a three-electrode configuration with a scan rate of 5 mV s^{-1}. As a contrast, three samples, NiCoP-8, NiCoP-16, and NiCoP-24, were tested, respectively. From Figure 4a, we can find that the NiCoP-16 displays an excellent HER property, which only needs a low overpotential of 57 mV to reach 10 mA cm^{-2}, much lower than NiCoP-8 (101 mV) and NiCoP-24 (129 mV). As depicted in Figure 4b, we can see that the Tafel slope of NiCoP-16 is 68 mV dec^{-1}, which is much lower than those of NF (98 mV dec^{-1}), NiCoP-8 (90 mV dec^{-1}), and NiCoP-24 (94 mV dec^{-1}). These results indicate that the HER process of NiCoP-16 follows the Volmer−Heyrovský mechanism. In order to understand the progress of the HER property of NiCoP-16, we measured the electrochemical active surfaces (ECSAs) via the double-layer capacitances (C_{dl}). The CV and its corresponding computational procedure are shown in Figure S4a−d. Figure S4e illustrates that the C_{dl} values of NF, NiCoP-8, NiCoP-16, and NiCoP-24 were calculated to be 0.68, 0.7, 4.18, and 0.88 mF cm^{-2}, respectively, indicating that NiCoP-16 boasts the highest ECSA and abundant active sites. Electrochemical impedance

https://doi.org/10.1021/acsomega.1c01650
ACS Omega 2021, 6, 26822−26828

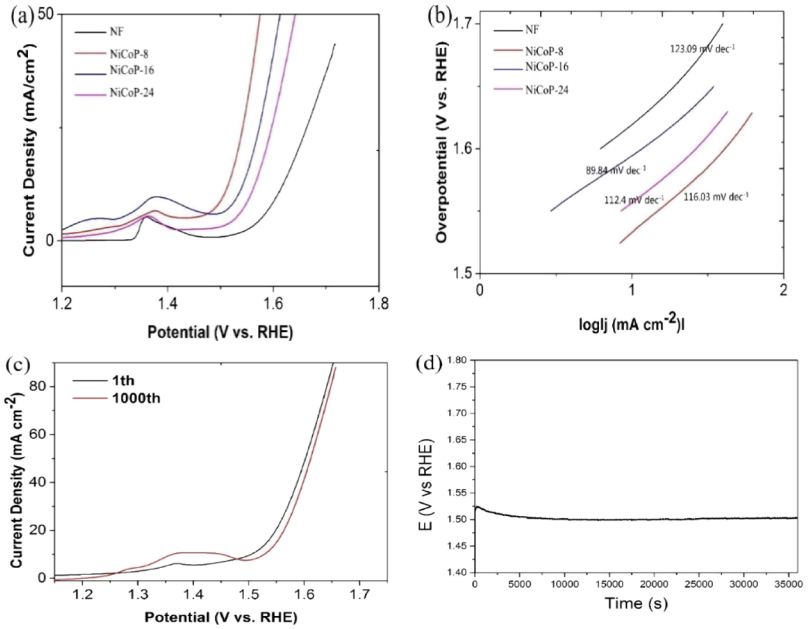

Figure 5. OER activities of the as-prepared electrocatalysts in H_2-saturated 1 M KOH. (a) Polarization curves recorded with a scan rate of 5 mV s^{-1}. (b) Tafel plots derived from (a). (c) OER stability test of NiCoP for 1000 potential cycles of CV. (d) CP curves of NiCoP.

spectroscopy is an effective method to study the electrode kinetics interface reactions of NF, NiCoP-8, NiCoP-16, and NiCoP-24 in the HER process, as evidenced by Figure S4f. Compared with the other three samples, the NiCoP-16 shows a smaller charge transfer resistance R_{ct} (6 Ω) than those of NF (78 Ω), NiCoP-8 (43 Ω), and NiCoP-24 (18 Ω), which implies the faster electron transfer and enhanced electrochemical performance for NiCoP-16 in HER.[58] The outstanding property of NiCoP-16 can give the credit to not only the special morphology but also the intrinsic electronic properties. The increase in the contact area between the electrolyte and interface, the shortening of ion/mass diffusion paths, and the acceleration of charge transfer are owed to the 3D hierarchical and loose structure.

In addition, designing a sustained and steady nanostructured electrocatalyst is of great significance for optimizing the catalytic property. From +0.2 to −0.2 V (vs RHE), the NiCoP-16 was further operated in successive CV tests with an accelerated scanning rate of 50 mV s^{-1}. The HER LSV curves show a tendency that is almost identical to the initial one after 1000 CV cycles (Figure 4c). The NiCoP-16 also exhibits excellent HER stability with a negligible potential degradation for long-term electrochemical tests (Figure 4d). Notably, the morphology of the NiCoP-16 catalyst is well-preserved after the durability measurement, as evinced by Figure S5a,b for their SEM images, showing an excellent structural durability to retain marvelous catalytic performance in cycling.

Moreover, in 1 M KOH solution, the OER performance of the NiCoP electrode was evaluated as well. Figure 5a shows LSV curves of these four electrodes with iR corrected. As illustrated, the NiCoP-16 boasts an optimal OER performance and only needs a relatively low overpotential of 276 mV to deliver a geometric current density of 10 mA cm^{-2}, outperforming NiCoP-8 (303 mV) and NiCoP-24 (327 mV). In addition, all the catalysts exhibit a clear anodized peak at about 1.35 V (vs RHE),[59] and this phenomenon may be related to the oxidation of Ni or Co (or both) species. According to the corresponding Tafel plots (Figure 5b), we evaluated the reaction kinetics. Compared with NiCoP-8 (112 mV dec^{-1}) and NiCoP-24 (116 mV dec^{-1}), NiCoP-16 (89 mV dec^{-1}) boasts the smallest Tafel slope. This indicates a more advantageous OER kinetics with a speed oxygen evolution rate. The relatively low small Tafel slope and onset potential emphasize the oxygen production efficiency of NiCoP-16, which places it at the top-tier electrocatalysts among other earth-abundant OER catalysts (Table S1). We tested the double-layer capacitance (C_{dl}) to calculate the ECSA to reveal the intrinsic catalytic property of NiCoP-16. The CV and its corresponding computational procedure are shown in Figure S6a−d. Figure S6e depicts that the C_{dl} of NiCoP-16 (6.45 mF cm^{-2}) is 1.3 and 1.8 times larger than that of NiCoP-8 (5.01 mF cm^{-2}) and NiCoP-24 (3.54 mF cm^{-2}), manifesting that more effective active sites are exposed. Via electrochemical impedance spectroscopy (Figure S6f), we further examined the electrode kinetics and interface reactions. Compared with the other two samples, as shown in the Nyquist plots, the NiCoP-16 electrocatalyst shows a smaller charge transfer resistance (R_{ct} = 2.76 Ω) than Ni foam (43.66 Ω), NiCoP-8 (3.98 Ω), and NiCoP-24 (4.53 Ω), indicating the faster electron transfer and enhanced electrochemical activity. The enhanced charge transfer property could facilitate the conjunction of H_{ads} and electrons, as well as profit electrical integration to diminish concomitant ohmic losses, which further leads to the enhanced electrocatalytic activity. Moreover, the stability of NiCoP-16 was examined by a continuous CV test and chronopotentiometry. The OER polarization curve for NiCoP-16 still retains the initial one and shows negligible decay after 1000 CV cycles (Figure 5c). Also, the NiCoP-16 exhibits satisfying stability (Figure 5d). The morphology of the post-cycling sample retains a similar structure to that of the as-synthesized NiCoP-16, except for the surface of nanowires consisting of the dandelion-like arrays covered by ultrathin nanosheets (Figure S7a,b). However, the ultrathin nanosheets are demonstrated to have a negligible effect on stability, as illustrated in Figure 5d.

Induced by the profound property of the three-dimensional dandelion-like NiCoP during the water splitting process, we

https://doi.org/10.1021/acsomega.1c01650
ACS Omega 2021, 6, 26822−26828

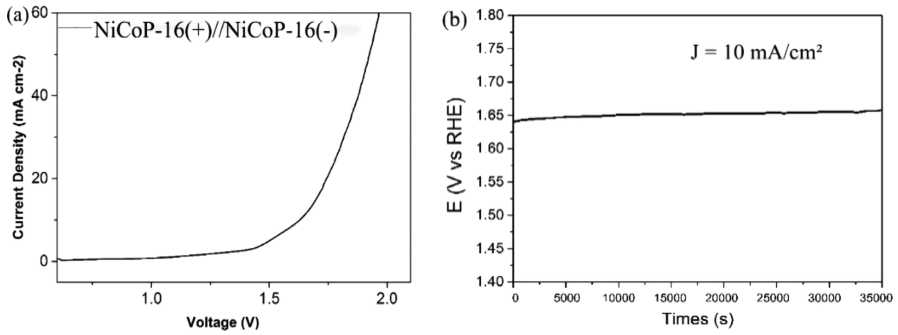

Figure 6. (a) Polarization curves of the NiCoP-16(+)//NiCoP-16(−) couple. (b) CP curves of the NiCoP-16(+)//NiCoP-16(−) couple.

used a NiCoP-16(+)//NiCoP-16(−) couple to assemble an alkane electrolyte. The overall water splitting property was evaluated by LSV. As can be seen, Figure 6a shows that the NiCoP-16 exhibits a high activity with a relatively low cell voltage of 1.63 V to afford 10 mA cm^{-2}. Moreover, the electrode demonstrates durability for overall water electrolysis well (Figure 6b).

CONCLUSIONS

To sum up, we have established NiCoP with dandelion-like arrays anchored on nanowires for more efficient water splitting. Owing to a series of advantages, such as enormous surface areas, affluent active sites, and low mass and charge transfer resistance, in the alkaline environment, the hierarchical NiCoP nanostructure catalyst exhibits excellent property and durability. It only needs relatively low overpotentials of 57 and 276 mV to afford 10 mA cm^{-2} for HER and OER, respectively. Furthermore, the NiCoP-16(+)//NiCoP-16(−) couple needs a cell voltage of 1.63 V to drive a current density of 10 mA cm^{-2}. This work elucidates that the elegant designs of morphology can pave the way of various complex transition metal-based materials for more energy applications, e.g., supercapacitors, battery electrodes, and electrocatalysis.

EXPERIMENTAL SECTION

Fabrication of NiCoP with Dandelion-like Arrays Anchored on Nanowires. We first produce the precursor (NiCo-pre) on nickel foam (NF) through a hydrothermal approach. Before reaction, the NF was thoroughly cleaned with acetone and water. After then, it was cut into several pieces (2 × 4 cm^2) for utilization. Nickel nitrate hexahydrate, cobalt nitrate hexahydrate, and urea were homogeneously dissolved in 30 mL of deionized water. The total concentration of the solution was 1.5 mM (the ratio of nickel salt to cobalt salt is 2:1). Then, the solution was transferred into a Teflon container. The NF was immersed into the solution. Subsequently, the container was sealed in an autoclave and heated at 120 °C for 16 h to obtain the precursor. As a control experiment, the precursor was also synthesized with a quarter concentration of the solution, which was denoted as NiCo-pre/4. In addition, the variance of reaction time will result in different morphologies of NiCo-pre. Therefore, the precursors were prepared at 120 °C for 8, 16, and 24 h, respectively.

Next, the prepared precursor was immersed in 40 mL of distilled water containing $NaH_2PO_2{\cdot}H_2O$ (24 mM) and together transferred to the same autoclave used in the first step. The reaction was maintained at 160 °C for 8 h. After a certain time of cooling, the NiCoP was obtained. The NiCoP-8, NiCoP-16, and NiCoP-24 represent the NiCoP derived from the NiCo-pre synthesized at the hydrothermal times of 8, 16, and 24 h, respectively, after phosphorization.

Characterization. The microstructure of the prepared materials was observed by field emission scanning microscopy (FESEM, FEI QUANTA 650) and transmission electron microscopy (TEM, JEOL 2100). The crystal phase was identified using powder X-ray diffraction (XRD-7000) and X-ray photoelectron spectroscopy (XPS, PHI5700 ESCA).

Electrochemical Tests. We used an electrochemistry workstation (CHI660, Shanghai) to evaluate electrocatalytic properties. In a three-electrode cell, the sample, a Pt wire, and a Hg/HgO electrode acted as the working, the counter, and the reference electrode, respectively. All the electrochemical tests (HER and OER) were conducted in a 1 M KOH electrolyte. Polarization curves were gathered with a scan rate of 2 mV s^{-1}. In all the measurements, we calibrate the reference electrode versus a reversible hydrogen electrode (RHE) based on the formula $E_{RHE} = E_{Hg/HgO} + 0.098 + 0.059pH$. The scanning rate of the CV curve during the stability test was 50 mV S^{-1} for 2000 cycles. The applied voltage of the impedance spectra is obtained at −0.1 V vs RHE for the HER and 1.6 V vs RHE for the OER in a frequency region of 0.1−10^5 Hz.

ASSOCIATED CONTENT

Supporting Information

The Supporting Information is available free of charge at https://pubs.acs.org/doi/10.1021/acsomega.1c01650.

Details of structural characterization and electrocatalytic properties of NiCoP materials and table comparing the previously reported HER and OER performance with the present study (PDF)

AUTHOR INFORMATION

Corresponding Author

Ailing Fan − *Key Laboratory of Advanced Functional Materials, Education Ministry of China, Beijing University of Technology, Beijing 100124, China;* orcid.org/0000-0002-8456-0296; Email: fanailing@bjut.edu.cn

Authors

Wei Pang − *Key Laboratory of Advanced Functional Materials, Education Ministry of China, Beijing University of Technology, Beijing 100124, China*

Yaqi Guo − *Key Laboratory of Advanced Functional Materials, Education Ministry of China, Beijing University of Technology, Beijing 100124, China*

https://doi.org/10.1021/acsomega.1c01650
ACS Omega 2021, 6, 26822−26828

Dengkui Xie − *Key Laboratory of Advanced Functional Materials, Education Ministry of China, Beijing University of Technology, Beijing 100124, China*

Dianchao Gao − *Key Laboratory of Advanced Functional Materials, Education Ministry of China, Beijing University of Technology, Beijing 100124, China*

Complete contact information is available at: https://pubs.acs.org/10.1021/acsomega.1c01650

Notes

The authors declare no competing financial interest.

■ ACKNOWLEDGMENTS

This work was supported by the National Natural Science Foundation of China (no. 22075290).

■ REFERENCES

(1) Zhou, X.; Liao, X.; Pan, X.; Yan, M.; He, L.; Wu, P.; Zhao, Y.; Luo, W.; Mai, L. Unveiling the Role of Surface P−O Group in P-doped Co_3O_4 for Electrocatalytic Oxygen Evolution by On-chip Micro-device. *Nano Energy* **2021**, *83*, 105748−105756.

(2) Yan, Y.; He, T.; Zhao, B.; Qi, K.; Liu, H.; Xia, B. Y. Metal/covalent-organic Frameworks-based Electrocatalysts for Water Splitting. *J. Mater. Chem. A* **2018**, *6*, 15905−15926.

(3) Xu, H.; Wei, J.; Zhang, K.; Shiraishi, Y.; Du, Y. Hierarchical NiMo Phosphide Nanosheets Strongly Anchored On Carbon Nanotubes as Robust Electrocatalysts for Overall Water Splitting. *ACS Appl. Mater. Interfaces* **2018**, *10*, 29647−29655.

(4) Li, Z.; Fu, J. Y.; Dong, C. K.; Liu, H.; Du, X. W. A Silver Catalyst Activated by Stacking Faults for the Hydrogen Evolution Reaction. *Nat. Catal.* **2019**, *2*, 1104−1114.

(5) Zhu, J.; Wang, Z.-C.; Dai, H.; Wang, Q.; Yang, R.; Yu, H.; Liao, M.; Zhang, J.; Chen, W.; Wei, Z.; Lin, N.; Du, L.; Shi, D.; Wang, W.; Zhang, L.; Jiang, Y.; Zhang, G. Boundary Activated Hydrogen Evolution Reaction on Monolayer MoS_2. *Nat. Commun.* **2019**, *10*, 1348−1355.

(6) Jiang, W. J.; Niu, S.; Tang, T.; Zhang, Q. H.; Liu, X. Z.; Zhang, Y.; Chen, Y. Y.; Li, J. H.; Gu, L.; Wan, L. J.; Hu, J. S. Crystallinity-modulated Electrocatalytic Activity of a Nickel(II) Borate Thin Layer on Ni_3B for Efficient Water Oxidation. *Angew. Chem., Int. Ed.* **2017**, *56*, 6572−6577.

(7) Wang, X.; Li, W.; Xiong, D.; Petrovykh, D. Y.; Liu, L. Bifunctional Nickel Phosphide Nanocatalysts Supported on Carbon Fiber Paper for Highly Efficient and Stable Overall Water Splitting. *Adv. Funct. Mater.* **2016**, *26*, 4067−4077.

(8) Shan, X.; Liu, J.; Mu, H.; Xiao, Y.; Mei, B.; Liu, W.; Lin, G.; Jiang, Z.; Wen, L.; Jiang, L. An Engineered Superhydrophilic/superaerophobic Electrocatalysts Composed of Supported $CoMoS_x$ Chalcogels for Overall Water Splitting. *Angew. Chem., Int. Ed.* **2020**, *59*, 1659−1665.

(9) Guo, M.; Zhou, L.; Li, Y.; Zheng, Q.; Xie, F.; Lin, D. Unique Nanosheet−nanowire Structured CoMnFe Layered Triple Hydroxide Arrays as Self-supporting electrodes for a High-efficiency Oxygen Evolution Reaction. *J. Mater. Chem. A* **2019**, *7*, 13130−13141.

(10) Wang, Z.; Zhang, Y.; Li, Y.; Fu, H. Hierarchical Porous $NiCo_2O_4$ Nanograss Arrays Grown on Ni Foam as Electrode Material for High-performance Supercapacitors. *RSC Adv.* **2014**, *4*, 20234−20238.

(11) Feng, H.; Xu, Z.; Ren, L.; Liu, C.; Zhuang, J.; Hu, Z.; Xu, X.; Chen, J.; Wang, J.; Hao, W.; Du, Y.; Dou, S. X. Activating Titania for Efficient Electrocatalysis by Vacancy Engineering. *ACS Catal.* **2018**, *8*, 4288−4293.

(12) Yu, Z. Y.; Lang, C. C.; Gao, M. R.; Chen, Y.; Fu, Q. Q.; Duan, Y.; Yu, S. H. Ni−Mo−O Nanorod-derived Composite Catalysts for Efficient Alkaline Water-to-hydrogen Conversion via Urea Electrolysis. *Energy Environ. Sci.* **2018**, *11*, 1890−1897.

(13) McEnaney, J. M.; Soucy, T. L.; Hodges, J. M.; Callejas, J. F.; Mondschein, J. S.; Schaak, R. E. Colloidally-Synthesized Cobalt Molybdenum Nanoparticles as Active and Stable Electrocatalysts for the Hydrogen Evolution Reaction Under Alkaline Conditions. *J. Mater. Chem. A* **2016**, *4*, 3077−3081.

(14) Liu, J.; Zheng, Y.; Jiao, Y.; Wang, Z.; Lu, Z.; Vasileff, A.; Qiao, S.-Z. NiO as a Bifunctional Promoter for RuO_2toward Superior Overall Water Splitting. *Small* **2018**, *14*, 1704073.

(15) Xu, Q.; Jiang, H.; Zhang, H.; Jiang, H.; Li, C. Phosphorus-driven Mesoporous Co_3O_4 Nanosheets with Tunable Oxygen Vacancies for the Enhanced Oxygen Evolution Reaction. *Electrochim. Acta* **2018**, *259*, 962−967.

(16) Benck, J. D.; Hellstern, T. R.; Kibsgaard, J.; Chakthranont, P.; Jaramillo, T. F. Catalyzing the Hydrogen Evolution Reaction (HER) with Molybdenum Sulfide Nanomaterials. *ACS Catal.* **2014**, *4*, 3957−3971.

(17) Swesi, A. T.; Masud, J.; Nath, M. Nickel Selenide as a High-efficiency Catalyst for Oxygen Evolution Reaction. *Energy Environ. Sci.* **2016**, *9*, 1771−1782.

(18) Gao, R.; Zhang, H.; Yan, D. Iron Diselenide Nanoplatelets: Stable and Efficient Water-electrolysis Catalysts. *Nano Energy* **2017**, *31*, 90−95.

(19) Wang, G.; Chen, W.; Chen, G. L.; Huang, J.; Song, C.; Chen, D.; Du, Y.; Li, C.; Ostrikov, K. K. Trimetallic Mo-Ni-Co Selennides Nanorod Electrocatalysts for Highly-efficient and Ultra-stable Hydrogen Evolution. *Nano Energy* **2020**, *71*, 104637−104648.

(20) Huang, Z.; Xu, B.; Li, Z.; Ren, J.; Mei, H.; Liu, Z.; Xie, D.; Zhang, H.; Dai, F.; Wang, R.; Sun, D. Accurately Regulating the Electronic Structure Ni_xSe_y@NC Core-shell Nanohybrids Through controllable Selenization of a Ni-MOF for pH-universal Hydrogen Evolution Reaction. *Small* **2020**, *16*, 2004231−2004242.

(21) Yu, J.; Cheng, G.; Luo, W. 3D Mesoporous Rose-like Nickel-iron Selenide Microspheres as Advanced Electrocatalysts for the Oxygen Evolution Reaction. *Nano Res.* **2018**, *11*, 2149−2158.

(22) Yang, Y.; Yu, H.; Islam, S. M.; He, H.; Yuan, M.; Yue, Y.; Xu, K.; Hao, W.; Sun, G.; Li, H.; Ma, S.; Zapol, P.; Kanatzidis, M. G. Hierarchical Nano Assembly of $MoS_2/Co_9S_8/Ni_3S_2$/Ni as a Highly Efficient Electrocatalyst for Overall Water Splitting in a Wide pH Range. *J. Am. Chem. Soc.* **2019**, *141*, 10417−10430.

(23) Lin, L.; Miao, N.; Wen, Y.; Zhang, S.; Ghosez, P.; Sun, Z.; Allwood, D. A. Sulfur-depleted Monolayered Molybdenum Disulfide Nanocrystals for Superelectrochemical Hydrogen Evolution Reaction. *ACS Nano* **2016**, *10*, 8929−8937.

(24) Deng, J.; Li, H.; Wang, S.; Ding, D.; Chen, M.; Liu, C.; Tian, Z.; Novoselov, K. S.; Ma, C.; Deng, D.; Bao, X. Multiscale Structural and Electronic Control of Molybdenum Disulfide Foam for Highly Efficient hydrogen Production. *Nat. Commun.* **2017**, *8*, 10933−10941.

(25) Li, Y.; Wang, H.; Xie, L.; Liang, Y.; Hong, G.; Dai, H. MoS_2 Nanoparticles Grown on Graphene: an Advanced Catalyst for the Hydrogen Evolution Reaction. *J. Am. Chem. Soc.* **2011**, *133*, 7296−7299.

(26) Lukowski, M. A.; Daniel, A. S.; English, C. R.; Meng, F.; Forticaux, A.; Hamers, R. J.; Jin, J. Highly Active Hydrogen Evolution Catalysis From Metallic WS_2 nanosheets. *Energy Environ. Sci.* **2014**, *7*, 2608−2613.

(27) Voiry, D.; Yamaguchi, H.; Li, J.; Silva, R.; Alves, D. C. B.; Fujita, T.; Chen, M.; Asefa, T.; Shenoy, V. B.; Eda, G.; Chhowalla, M. Enhanced Catalytic Activity in Strained Chemically Exfoliated WS_2 Nanosheets for Hydrogen Evolution. *Nat. Mater.* **2013**, *12*, 850−855.

(28) Yu, L.; Zhu, Q.; Song, S.; McElhenny, B.; Wang, D.; Wu, C.; Qin, Z.; Bao, J.; Yu, Y.; Chen, S.; Ren, Z. Non-noble Metal-nitride Based Electrocatalysts for High-performance Alkaline Seawater Electrolysis. *Nat. Commun.* **2019**, *10*, 5106−5116.

(29) Mishra, I. K.; Zhou, H.; Sun, J.; Qin, F.; Dahal, K.; Bao, J.; Chen, S.; Ren, Z. Hierarchical CoP/Ni_5P_4/CoP Microsheet Arrays as a Robust pH-universal Electrocatalyst for Efficient Hydrogen Generation. *Energy Environ. Sci.* **2018**, *11*, 2246−2252.

(30) Shi, Y.; Zhang, B. Recent Advances in Transition Metal Phosphide Nanomaterials: Synthesis and Applications in Hydrogen Evolution Reaction. *Chem. Soc. Rev.* **2016**, *45*, 1529−1541.
(31) Wu, R.; Xiao, B.; Gao, Q.; Zheng, Y. R.; Zheng, X. S.; Zhu, J. F.; Gao, M. R.; Yu, S. H. A Janus Nickel Cobalt Phosphide Catalyst for High-efficiency Neutral-pH Water Splitting. *Angew. Chem., Int. Ed.* **2018**, *57*, 15445−15449.
(32) Li, Y.; Dong, Z.; Jiao, L. Multifunctional Transition Metal-based Phosphides in Energy-related Electrocatalysis. *Adv. Energy Mater.* **2020**, *10*, 1902104−1902140.
(33) Li, X.; Zhang, R.; Luo, Y.; Liu, Q.; Lu, S.; Chen, G.; Gao, S.; Chen, S.; Sun, X. A Cobalt-phosphorous Nanoparticle Decorated N-doped Carbon Nanosheet Array for Efficient and Durable Hydrogen Evolution at Alkaline pH. *Sustain. Energy Fuels* **2020**, *4*, 3884−3887.
(34) Liu, T.; Xie, L.; Yang, J.; Kong, R.; Du, G.; Asiri, A. M.; Sun, X.; Chen, L. Self-Standing CoP Nanosheets Array: A Three-Dimensional Bifunctional Catalyst Electrode for Overall Water Splitting in both Neutral and Alkaline Media. *ChemElectroChem* **2017**, *4*, 1840−1845.
(35) Liu, T.; Liu, D.; Qu, F.; Wang, D.; Zhang, L.; Ge, R.; Hao, S.; Ma, Y.; Du, G.; Asiri, A. M.; Chen, L.; Sun, X. Enhanced Electrocatalysis for Energy-Efficient Hydrogen Production over CoP Catalyst with Nonelectroactive Zn as a Promoter. *Adv. Energy Mater.* **2017**, *7*, 1700020.
(36) Zhang, L.; Ren, X.; Guo, X.; Liu, Z.; Asiri, A. M.; Li, B.; Chen, L.; Sun, X. Efficient Hydrogen Evolution Electrocatalysis at Alkaline pH by Interface Engineering of Ni_2P−CeO_2. *Inorg. Chem.* **2018**, *57*, 548−552.
(37) Liu, S.; Chen, Y.; Yu, L.; Lin, Y.; Liu, Z.; Wang, M.; Chen, Y.; Zhang, C.; Pan, Y.; Liu, Y.; Liu, C. A Supramolecular-confinement Pyrolysis Route to Ultrasmall Rhodium Phosphide Nanoparticles as a Robust Electrocatalyst for Hydrogen Evolution in the Entire pH Range and Seawater Electrolysis. *J. Mater. Chem. A* **2020**, *8*, 25768−25779.
(38) Wu, K.; Sun, K.; Liu, S.; Cheong, W.-C.; Chen, Z.; Zhang, C.; Pan, Y.; Cheng, Y.; Zhuang, Z.; Wei, X.; Wang, Y.; Zheng, L.; Zhang, Q.; Wang, D.; Peng, Q.; Chen, C.; Li, Y. Atomically Dispersed Ni−Ru−P Interface Sites for High-Efficiency pH-Universal Electrocatalysis of Hydrogen Evolution. *Nano Energy* **2021**, *80*, 105467.
(39) Xiao, P.; Chen, W.; Wang, X. A Review of Phosphide-based Materials for Electrocatalytic Hydrogen Evolution. *Adv. Energy Mater.* **2015**, *5*, 1500985−1500998.
(40) Liu, K.; Wang, F.; Shifa, T. A.; Wang, Z.; Xu, K.; Zhang, Y.; Cheng, Z.; Zhan, X.; He, J. An Efficient Ternary $CoP_{2x}Se_{2(1-x)}$ Nanowire Array for Overall Water Splitting. *Nanoscale* **2017**, *9*, 3995−4001.
(41) Ma, X. X.; Dai, X. H.; He, X. Q. Co_9S_8-modified N, S, and P ternary-doped 3D Graphene Aerogels as a High-performance Electrocatalyst for Both the Oxygen Reduction Reaction and Oxygen Evolution reaction. *ACS Sustainable Chem. Eng.* **2017**, *5*, 9848−9857.
(42) Du, C.; Yang, L.; Yang, F.; Cheng, G.; Luo, W. Nest-like NiCoP for Highly Efficient Overall Water Splitting. *ACS Catal.* **2017**, *7*, 4131−4137.
(43) Wagner, A.; Sahm, C. D.; Reisner, E. Towards Molecular Understanding of Local Chemical Environment Effects in Electro- and Photocatalytic CO_2 Reduction. *Nat. Catal.* **2020**, *3*, 775−786.
(44) Klingenhof, M.; Hauke, P.; Brückner, S.; Dresp, S.; Wolf, E.; Nong, H. N.; Spöri, C.; Merzdorf, T.; Bernsmeier, D.; Teschner, D.; Schlögl, R.; Strasser, P. Modular Design of Highly Active Unitized Reversible Fuel Cell Electrocatalysts. *ACS Energy Lett.* **2021**, *6*, 177−183.
(45) Shi, F.; Zhu, X.; Yang, W. Micro-nanostructural Designs of Bifunctional Electrocatalysts for Metal-air Batteries. *Chin. J. Catal.* **2020**, *41*, 390−403.
(46) Xie, Y.; Qian, Q.; Zhang, J.; Li, J.; Li, Y.; Jin, X.; Zhu, Y.; Liu, Y.; Li, Z.; El-Harairy, A.; Xiao, C.; Zhang, G. Artificial Hetero-interfaces Achieve Delicate Reaction Kinetics towards Hydrogen Evolution and Hydrazine Oxidation Catalysis. *Am. Ethnol.* **2021**, *133*, 2−6058.
(47) Pan, Y.; Zhang, C.; Lin, Y.; Liu, Z.; Wang, M.; Chen, C. Electrocatalyst Engineering and Structure-activity Relationship in Hydrogen Evolution Reaction: From Nanostructures to Single Atoms. *Sci. China Mater.* **2020**, *63*, 921−948.
(48) Ahsan, M. A.; He, T. W.; Abdullah, A. M.; Curry, M. L.; Du, A. J.; Santiago, A. R. P.; Echegoyen, L.; Noveron, J. C. Tuning the Intermolecular Electron Transfer of Low-dimensional and Metal-free BCN/C_{60} Electrocatalysts via Interfacial Defects for Efficient Hydrogen and Oxygen Electrochemistry. *J. Am. Chem. Soc.* **2021**, *143*, 1203−1215.
(49) Li, J.; Zheng, G. One-dimensional Earth-abundant Nanomaterials For water-splitting Electrocatalysts. *Adv. Sci.* **2017**, *4*, 1600380−1600395.
(50) Zhang, L.; Zhao, H.; Xu, S.; Liu, Q.; Li, T.; Luo, Y.; Gao, S.; Shi, X.; Asiri, A. M.; Sun, X. Recent Advances in 1D Electrospun Nanocatalysts for Electrochemical Water Splitting. *Small Struct* **2021**, *2*, 2000048.
(51) Yan, L.; Xu, Y.; Chen, P.; Zhang, S.; Jiang, H.; Yang, L.; Wang, Y.; Zhang, L.; Shen, J.; Zhao, X.; Wang, L. A Freestanding 3D Heterostructure Film Stitched by MOF-Derived Carbon Nanotube Microsphere Superstructure and Reduced Graphene Oxide Sheets: a Superior Multifunctional Electrode for Overall Water Splitting and Zn−Air Batteries. *Adv. Mater.* **2020**, *32*, 2003313−2003324.
(52) Huang, C.; Wu, D.; Qin, P.; Ding, K.; Pi, C.; Ruan, Q.; Song, H.; Gao, B.; Chen, H.; Chu, P. K. Ultrafine Co Nanodots Embedded in N-doped Carbon Nanotubes Grafted on Hexagonal VN for Highly Efficient Overall Water Splitting. *Nano Energy* **2020**, *73*, 104788−104796.
(53) Wang, H.; Wang, H.; Wang, Z.; Tang, L.; Zeng, G.; Xu, P.; Chen, M.; Xiong, T.; Zhou, C.; Li, X.; Huang, D.; Zhu, Y.; Wang, Z.; Tang, J. Covalent Organic Framework Photocatalysts: Structures and Applications. *Chem. Soc. Rev.* **2020**, *49*, 4135−4165.
(54) Liu, X.; Meng, J.; Ni, K.; Guo, R.; Xia, F.; Xie, J.; Li, X.; Wen, B.; Wu, P.; Li, M.; Wu, J.; Wu, X.; Mai, L.; Zhao, D. Complete Reconstruction of Hydrate Precatalysts for Ultrastable Water Electrolysis in Industrial-concentration Alkali Media. *Cell Rep. Phys. Sci.* **2020**, *1*, 100241−100258.
(55) Song, W.; Li, M.; Wang, C.; Lu, X. Electronic Modulation and Interface Engineering of Electrospun Nanomaterials-based Electrocatalysts toward Water Splitting. *Carbon Energy* **2021**, *3*, 101−128.
(56) Ishikawa, H.; Sheng, M.; Nakata, A.; Nakajima, K.; Yamazoe, S.; Yamasaki, J.; Yamaguchi, S.; Mizugaki, T.; Mitsudome, T. Air-stable and Reusable Cobalt Phosphide Nano Alloy Catalyst for Selective Hydrogenation of Furfural Derivatives. *ACS Catal.* **2021**, *11*, 750−757.
(57) Xia, M.; Liu, Y.; Wei, Z.; Chen, S.; Xiong, K.; Li, L.; Ding, W.; Hu, J.; Wan, L.-J.; Li, R.; Alvia, S. F. Pd-induced Pt(IV) Reduction to Form Pd@Pt/CNT Core@shell Catalyst for a more complete Oxygen Reduction. *J. Am. Chem. Soc.* **2013**, *1*, 14443−11448.
(58) Li, Z.; Yang, J.; Chen, Z.; Zheng, C.; Wei, L. Q.; Yan, Y.; Hu, H.; Wu, M.; Hu, Z. V "Bridged" Co-O to Eliminate Charge Transfer Barriers and Drive Lattice Oxygen Oxidation During Water-splitting. *Adv. Funct. Mater.* **2021**, *31*, 2008822−2008830.
(59) Lu, J.; Yue, J.-N.; Xiong, L.; Wang, X.; Zhang, W.-K.; Chen, L.; Wu, L.-M. Uniform Alignment of Non-π-conjugated Species Enhances Deep Ultraviolet Optical Nonlinearity. *J. Am. Chem. Soc.* **2019**, *141*, 8093−8097.

https://doi.org/10.1021/acsomega.1c01650
ACS Omega 2021, 6, 26822−26828